Structural, morphological and optical characterization of CdS-doped silica aerogels synthesized through sol-gel method

Materials Research Bulletin 192 (2025) 113590

Contents lists available at ScienceDirect

Materials Research Bulletin

journal homepage: www.elsevier.com/locate/matresbu

Research Papers

Structural, morphological and optical characterization of CdS-doped silica aerogels synthesized through sol-gel method

Prashant B. Lihitkar [a], Sonali Kale [b], Rakesh A. Afre [c], Diego Pugliese [d,*]

[a] Department of Chemistry, Lokmanya Tilak Mahavidyalaya, Wani, Yavatmal, 445 304, India
[b] Department of Applied Sciences and Humanities, Pimpri Chinchwad College of Engineering, Nigdi, Pune, 411 004, India
[c] Department of Engineering Science, Zeal College of Engineering and Research, Narhe, Pune, 411 041, India
[d] National Institute of Metrological Research (INRiM), Torino, 10135, Italy

ARTICLE INFO

Keywords:
CdS nanocrystals
Silica aerogel
Sol-gel synthesis
Supercritical drying
Photoluminescence

ABSTRACT

Aerogels are highly porous materials characterized by ultra-low density. The incorporation of luminescent materials into silica aerogels results in luminescent aerogels, which have potential applications in light-emitting diodes and optoelectronic devices. In this study, the photoluminescence properties of CdS-doped silica aerogels are reported. The CdS-doped silica aerogels exhibited three distinct emission bands in the blue, green, and red regions. The blue emission is attributed to localized trap states on the CdS surface, while the green emission is associated with sulfur and cation vacancies. The red emission is linked to the substitution of sulfur traps by other counter ions. Supercritical drying of the CdS-doped aerogels resulted in the removal of quantum dots, indicating the non-covalent bonding of CdS nanoparticles to the silica matrix. However, a fraction of the quantum dots remained embedded in the aerogel, as evidenced by weak emission bands and the X-ray diffraction patterns of CdS nanocrystals.

1. Introduction

Aerogels are highly porous materials recognized as the lightest solid materials in the world. They exhibit low density (0.03 to 0.8 g/cm^3), high porosity (>90 %), and a wide range of open pore sizes. Silica aerogels, in particular, are optically transparent, and possess low thermal and acoustic conductivity. These unique properties make them highly suitable for applications in catalysis, particle and protein immobilization, nanoparticles synthesis, surface coatings, and separation technologies [1–3].

Over time, the synergy between nanoparticles and silica aerogels has attracted significant scientific interest. The fabrication of silica aerogel-based composites using novel methods has opened promising pathways for enhancing functionality. Notably, integrating nanoparticles into silica matrices has led to improved performance in fields such as sensing, catalysis, and photonics [4,5].

Silica aerogels can be doped with metals, semiconductors, or dyes during the gel formation process. Care must be taken during doping to ensure that the chemistry of gel formation remains undisturbed and that the properties of the dopant remain intact after aerogel formation. For example, Zhao et al. generated clusters of doped silica aerogels by incorporating carbon and Rh6G dye using a laser ablation method [6]. Other studies have explored the inclusion of aluminum oxide [7], graphene oxide [8–10], gold nanospheres, silver nanoplatelets, and CdSe/CdS core-shell quantum dots (QDs) [11]. Yi et al. [12] investigated composites of tetrapod-like ZnO (T-ZnO) with silica aerogels prepared via the sol-gel method. Using nitrobenzene as a model pollutant, they demonstrated that SiO_2 aerogel loading enhanced T-ZnO adsorption, thereby improving photocatalytic efficiency. Sorensen et al. [13] developed low-density CdSe-ZnS nanoparticle-doped silica aerogels, which exhibited high luminescence, visible light transmittance (68 %), and a large surface area (790 m^2/g).

Rai et al. [14] studied the influence of CdS on Tb^{3+}-doped glass using ultraviolet-visible (UV–Vis) and luminescence spectroscopy, reporting a significant enhancement in luminescence intensity in the presence of CdS nanoparticles. Mu et al. [15] investigated the optical properties of CdS-doped silica xerogels and observed that doping with CdS nanocrystals enhanced the photoluminescence (PL) of the silica xerogels. De La Rosa-Fox et al. [16] synthesized CdS semiconductor nanocrystals as QDs within a silica matrix using the sol-gel method. Their PL study at room temperature (RT) revealed radiative processes from intrinsic transitions and a broad band corresponding to trap states. Ben Slimen

* Corresponding author.
E-mail address: d.pugliese@inrim.it (D. Pugliese).

https://doi.org/10.1016/j.materresbull.2025.113590
Received 17 February 2025; Received in revised form 9 May 2025; Accepted 31 May 2025
Available online 31 May 2025

et al. [17] examined the effect of co-doping with CdS nanoparticles on the PL properties of Eu^{3+}-doped silico-phosphate glass prepared via the sol-gel method.

Bokatial et al. [18] embedded CdS nanoparticles along with Eu^{3+} ions in silica xerogels using the sol-gel technique. Their results showed that doping CdS nanoparticles enhanced the luminescence properties of Eu^{3+} even in the gel stage. Pei et al. [19] synthesized heterojunction structures comprising silica, CdS, and BiOX (X = Br, Cl) using a combination of mixed-solvent thermal treatment and ultrasonic deposition. The incorporation of CdS into the silica-BiOX matrix notably enhanced photocatalytic degradation performance. More recently, Fatemipayam et al. [20] investigated the synergistic effects of CdS and TiO_2 nanoparticles integrated into the porous framework of MCM-41. Their results demonstrated an optimal balance of visible-light absorption, efficient charge separation, and preservation of mesoporous structure, leading to highly effective photocatalytic activity.

Kaushik et al. [21] decorated CdS surfaces with functionalized graphene aerogels, imparting photocatalytic activity for the degradation of toxic Congo red dye under sunlight. Mohanan et al. [22] prepared aerogels composed of interconnected networks of CdS building blocks through controlled aggregation of discrete nanoparticles and supercritical fluid extraction. Prasad et al. [23] studied the photocatalytic activities of carbon aerogel-assisted CdS nanocomposites under visible light for the degradation of methylene blue and phenol. Yang et al. [24] synthesized metal–organic framework aerogels (MOAs) embedded with CdS (CdS/MOA(Cr)) via a facile one-pot solvothermal method and demonstrated their photocatalytic activity. Ikram et al. [25] synthesized carbon spheres doped with CdS QDs using a co-precipitation method, applying them for catalytic reduction and antibacterial applications.

The formation of aerogels has traditionally been limited to metal oxides and carbon due to challenges in gel formation. However, the development of aerogels from metal chalcogenides, such as CdS, ZnS, and CdSe, has introduced a novel approach to creating aerogels from luminescent semiconductor materials [26]. The essential requirement for chalcogenide aerogel formation is the ability to form a gel, which is a challenging process. The sol-gel chemistry of CdS colloids has been studied by Gacoin et al. [27]. Although aerogels from metal chalcogenides have been successfully prepared, the gel formation process is complex, requiring precise control of oxidant concentration and high nanoparticle concentrations. Unlike silica aerogels, hydrolysis does not work with chalcogenides, and stabilizing the gel is a significant challenge. Chalcogenide aerogels are typically prepared in three steps: thiolysis, nanoparticle condensation, and metathesis reactions between soluble chalcogenide clusters and linking metal ions [28]. During this process, nanoparticle condensation occurs through the controlled oxidation of thiolate anions. If the oxidant concentration is suboptimal, nanoparticle condensation will not occur, while excessive oxidant concentrations result in nanoparticle precipitation [29].

To address these challenges, in this study thiolate-capped CdS nanoparticles were synthesized using a microemulsion method [30–32] and subsequently added to a silica solution prior to gel formation to ensure uniform nanoparticle dispersion within the gel. Although the probability of covalent bonding between CdS nanoparticles and the silica matrix is low, thiolate anions enhanced the CdS network, supporting gel formation. The resulting CdS-doped silica aerogels were dried under ambient conditions as well as at the critical temperature of the solvent (supercritical drying). It was observed that the CdS dopant retained its luminescent properties after aerogel formation, and the aerogel chemistry remained unaffected by the dopant. This method provides a simple and effective approach to synthesizing CdS-doped silica aerogels. To the best of our knowledge, this is the first report of such a synthesis, which holds significant potential for aerogel-based technologies.

2. Experimental

2.1. Materials

Bis(2-ethylhexyl)sulfosuccinate sodium salt (AOT, Aldrich, 98 %), sodium sulfide (Na_2S, CDH India, AR grade), cadmium nitrate ($Cd(NO_3)_2$, CDH India, AR grade), 4-fluorobenzenethiol (Aldrich, 98 %), triethylamine (CDH India, AR grade), n-heptane (CDH India, AR grade), tetraethyl orthosilicate (TEOS, Merck India), ammonium fluoride (NH_4F, Thomas Baker, AR grade), and ammonia solution (Thomas Baker, 25 % aqueous) were used as received without further purification. Milli-Q water was used throughout the experiments.

2.2. Methodology

2.2.1. Synthesis of CdS nanoparticles

CdS nanoparticles were synthesized using the microemulsion method as reported in previous studies [31,32]. In a typical reaction, 11.15 g of AOT were dissolved in 48 mL of n-heptane to form a clear solution. This solution was divided into two parts. In part I, 1.12 mL of 0.15 M aqueous Na_2S solution was added and stirred for 15 min. Similarly, in part II, 1.12 mL of 0.15 M aqueous $Cd(NO_3)_2$ solution was added dropwise and stirred for 15 min to obtain a homogeneous solution. The two parts were then combined and stirred for 45 min. Subsequently, 1.8 mL of 4-fluorobenzenethiol and 2.2 mL of triethylamine were added dropwise to the mixture, which was stirred for an additional hour. A yellow precipitate was obtained, which was centrifuged and washed with n-heptane to remove excess AOT. The washed precipitate was dispersed in 2 mL of acetone to produce a homogeneous CdS colloidal solution.

2.2.2. Synthesis of CdS-doped silica aerogels

Silica aerogels were prepared using a standard sol-gel method [1]. In this process, 7 mL of H_2O, 7.5 mL of ethanol (C_2H_5OH), 0.03 mL of ammonia solution (NH_3), and 0.1 mL of 0.1 M NH_4F were mixed and stirred for 15 min at RT. Subsequently, 5.0 mL of TEOS were added slowly to control the gel formation. After stirring for 30–45 min, the silica sol became transparent. At this stage, 1 mL of the CdS colloidal solution was added to the silica sol, and the mixture was stirred briefly. The resulting mixture was poured into a plastic container and allowed to form a gel. After two days, the gel was removed from the container and soaked in ethanol to remove unreacted precursors. The CdS-doped silica gel was dried under two different conditions: (1) at ambient temperature (RT) and (2) under supercritical drying conditions at 260 °C.

The same procedure was repeated by doping the silica sol with 2 mL of CdS colloidal solution. The two different CdS doping concentrations, corresponding to the addition of 1 and 2 mL of CdS colloidal solution to the silica sol, are respectively denoted as C1 and C2 hereinafter.

2.3. Characterization

The optical properties of the colloidal CdS nanoparticles were analyzed using a PerkinElmer Lambda 950 UV–Vis spectrometer and a PerkinElmer LS-55 PL spectrophotometer. For the CdS-doped silica aerogels, powder samples were prepared for UV–Vis and PL spectral analyses. The crystalline structure of the CdS-doped aerogels was examined through X-ray diffraction (XRD) with a D8 Advanced Bruker X-ray diffractometer (CuK_α radiation, $\lambda = 1.54$ Å). Fourier transform infrared (FTIR) spectra were recorded using a Thermo Scientific Nicolet 6700 spectrometer. The samples were mixed with potassium bromide (KBr), which served as the reference matrix for IR analysis. The morphology of the CdS-doped silica aerogels was studied using a JEOL 6360-A scanning electron microscope (SEM). Thin films of the samples were prepared on clean silicon wafers for SEM analysis. Elemental analysis was carried out using the energy-dispersive X-ray spectrometer (EDS) integrated with the SEM, enabling detection and quantification of

Cd^{2+} and S^{2-} ions within the aerogel matrix.

3. Results and discussion

Aerogels are highly porous materials with a porosity exceeding 90 %, containing pores of variable sizes ranging from micropores (<2 nm) to macropores (>50 nm). In our work, CdS nanoparticles were synthesized using a microemulsion method known to yield highly monodispersed particles (~2 nm in size), minimizing the initial propensity for aggregation. The nanoparticles were then dispersed in a small volume of acetone to form a well-homogenized colloidal solution, which was then introduced into the silica sol when the gel precursors were still in a fluid state. Vigorous stirring at this stage ensured thorough mixing prior to gelation, facilitating a uniform distribution of nanoparticles within the forming silica network. The timing of the CdS nanoparticles incorporation was carefully optimized: the CdS colloid was added to a transparent, pre-gel silica sol to promote effective embedding of the nanoparticles within the growing gel matrix. This approach minimizes phase separation or clustering during gel formation. The optical properties of the CdS nanoparticles were characterized before their incorporation into the silica aerogel.

Fig. 1 presents the UV–Vis absorption and emission spectra of the CdS nanoparticles. The sharp absorption peak at 362 nm indicates the homogeneity and monodispersity of the confined CdS nanoparticles. The particle size, calculated from the absorption spectra using the effective mass approximation, was determined to be approximately 2 nm. The emission spectrum, recorded at an excitation wavelength of 362 nm, exhibits a prominent blue emission band at ~470 nm, as shown in Fig. 1. This emission is primarily attributed to localized surface trap states present on the surface of the CdS nanocrystals [31,32]. After gel formation, the samples were dried under two conditions: at RT (ambient drying) and at the supercritical temperature of the solvent (supercritical drying). The aerogel dried at RT with the lower concentration of CdS (C1) appeared opaque and exhibited a higher density of 1.2 g/cm^3, whereas the aerogel with the higher concentration of CdS (C2) was transparent and had a lower density of 0.8 g/cm^3 (see Table 1).

The supercritically dried CdS-silica aerogel, with a significantly lower density of 0.2 g/cm^3, showed a reduced presence of CdS nanocrystals (see Fig. 2). This observation suggests the removal of CdS nanoparticles during the supercritical drying process at the critical temperature of ethanol (260 °C). Additionally, the supercritically dried aerogel was found to be more fragile compared to the aerogels dried under ambient conditions.

The partial removal of CdS nanoparticles during supercritical drying

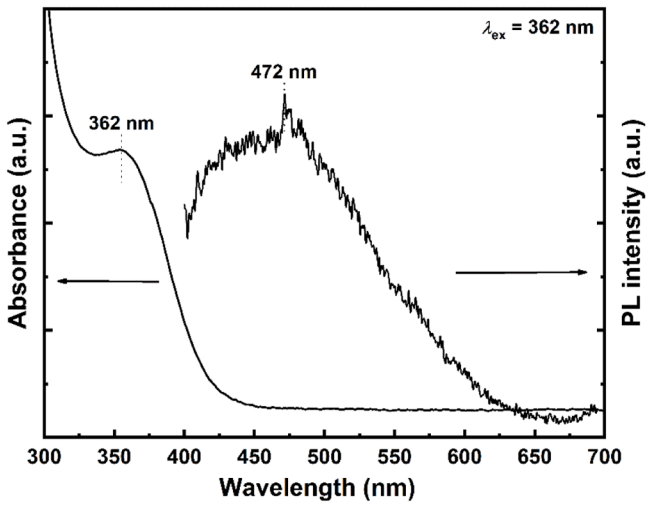

Fig. 1. UV–Vis and emission spectra of CdS nanoparticles. Excitation was performed at λ = 362 nm, emission was filtered at λ = 390 nm.

Table 1
Appearance and density values of different types of CdS-doped silica aerogels with C1 and C2 concentrations of CdS nanoparticles.

Aerogel	Drying	Appearance	Density (g/cm^3)
A) CdS-silica aerogel	Subcritical (Conc. C1)	Opaque	1.2
B) CdS-silica aerogel	Subcritical (Conc. C2)	Transparent	0.8
C) CdS-silica aerogel	Supercritical (Conc. C1)	Transparent	0.2
D) Silica aerogel	Subcritical	Transparent	0.7

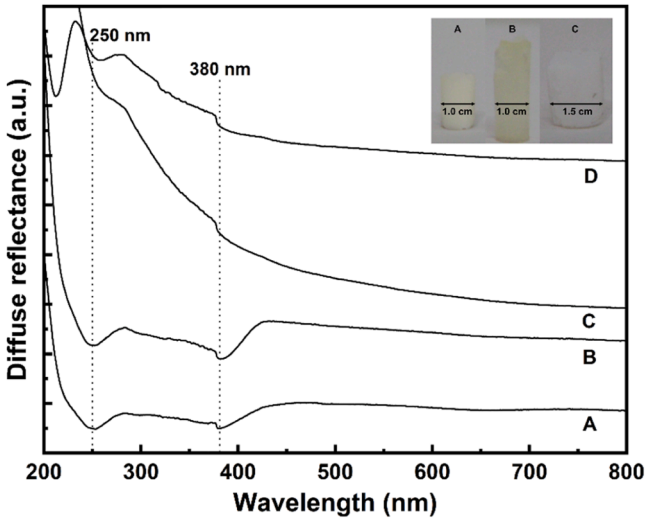

Fig. 2. UV–Vis diffuse reflectance spectra of CdS-silica aerogels (A-C) and undoped silica aerogel (D). Inset shows the picture images of CdS-doped silica aerogels for samples A, B and C.

can be rationalized by considering both thermodynamic and kinetic factors. Under supercritical conditions (~260 °C for ethanol), the solvent has negligible surface tension, eliminating the capillary forces that would normally help retain nanoparticles within the porous silica network. This makes nanoparticles that are held primarily by weak non-covalent interactions—such as Van der Waals forces and hydrogen bonding—more prone to desorption and loss.

From a thermodynamic perspective, the free energy balance of the system is significantly altered during supercritical drying. The Gibbs free energy change $\Delta G = \Delta H - T\Delta S$, where ΔH is the enthalpy change related to nanoparticle-matrix interactions, T is the absolute temperature, and ΔS is the entropy change of the system, is influenced by elevated temperatures and the unique solvent properties in the supercritical state [33]. Under these conditions, the thermal energy k_BT, where k_B is the Boltzmann constant, may approach or exceed the adsorption energies that stabilize the CdS-silica interface, thereby promoting nanoparticles desorption. Additionally, the absence of a liquid-vapor interface eliminates the associated interfacial energy penalty, further facilitating the release of CdS nanoparticles from the porous silica network.

From a kinetic standpoint, the high diffusivity and significantly reduced viscosity of the solvent in the supercritical phase enable rapid transport through the porous silica network. This dynamic flow can generate shear forces sufficient to disrupt the relatively weak non-covalent interactions anchoring CdS nanoparticles, effectively dislodging them from the pore structure before stable binding can be re-established. In contrast, under ambient drying conditions, the slower rate of solvent evaporation allows more time for these interactions to stabilize, leading to greater retention of CdS QDs within the silica matrix.

For clarity, the following nomenclature is used for the samples:

- Sample A: Subcritically dried aerogel with C1 concentration of CdS.

- Sample B: Subcritically dried aerogel with C2 concentration of CdS.
- Sample C: Supercritically dried aerogel with C1 concentration of CdS.
- Sample D: Subcritically dried silica aerogel without CdS doping.

Fig. 2 shows the UV–Vis diffuse reflectance spectra of the CdS-doped silica aerogels (A-C) and of the undoped silica aerogel (D). The peak at 380 nm in the subcritically dried CdS-silica aerogels corresponds to monodispersed CdS nanoparticles, which are confined within the pores of the silica aerogel. A characteristic spectral shift, indicative of quantum confinement and nanoparticles monodispersity, confirms their successful incorporation into the silica matrix. Curve D represents the subcritically dried silica aerogel without CdS doping. The silica aerogel exhibits a diffuse reflectance peak at 260 nm, which shifts to 250 nm in the CdS-silica aerogels (curves A and B). This shift may be attributed to the substitution of oxygen vacancies on the silica surface by S^{2-} anions during the drying process at RT. This effect is more pronounced in sample A, as evidenced by the higher intensity of the peak at 250 nm compared to the peak at 380 nm. This observation is likely due to the higher concentration of CdS nanoparticles in sample A, which causes greater contraction of the silica network, resulting in the opaque appearance of the aerogel. In contrast, these defects are not observed in sample C. At high temperatures, the solvent present in the pores of the gel is replaced by air, leading to the removal of CdS nanoparticles from the pores and the absence of oxygen defects.

The inset of Fig. 2 shows photographic images of the CdS-doped silica aerogels (A-C). Sample A appears opaque and pale yellow, while sample B is transparent with a light-yellow color, indicating the presence of CdS nanoparticles. Sample C, on the other hand, is almost white and transparent, suggesting the removal of CdS nanoparticles during the high-temperature supercritical drying process.

Elemental analysis performed using SEM-EDS (Table 2) confirms the presence of Cd^{2+} and S^{2-} ions in all CdS-doped silica aerogels (samples A-C). The Cd^{2+}/S^{2-} atomic ratio is approximately 1 in all samples except for sample B, regardless of the drying method. Notably, sample B, which was prepared with a higher concentration of CdS nanoparticles and subcritically dried, exhibits a Cd^{2+}/S^{2-} ratio close to 2. This excess of Cd^{2+} ions may influence the PL behavior, potentially altering the emission characteristics.

The crystallinity of the CdS nanocrystals in the CdS-silica aerogels was studied using XRD analysis, as shown in Fig. 3. The broad peaks in the XRD patterns of samples A-C are attributed to hexagonal CdS [31,32], confirming the presence of CdS nanocrystals within the silica aerogel. The diffraction planes (110), (103), (112), and (203) correspond to hexagonal CdS nanocrystals and are more prominent in samples A and B. In sample C, only the (103) plane of hexagonal CdS is observed, indicating the presence of a small amount of CdS QDs after supercritical drying. The XRD pattern of the amorphous silica aerogel (sample D) does not match the XRD patterns of the CdS-doped silica aerogels (A-C), further confirming the presence of CdS nanocrystals in the doped samples.

To investigate the covalent and non-covalent interactions within the CdS-doped silica aerogels, FTIR spectroscopy was performed on all samples A-D, as shown in Fig. 4. The corresponding peak positions and their assignments are summarized in Table 3. The FTIR spectra reveal a range of vibrational frequencies indicative of covalent bonding between CdS nanoparticles and the silica network. Notably, additional bands in

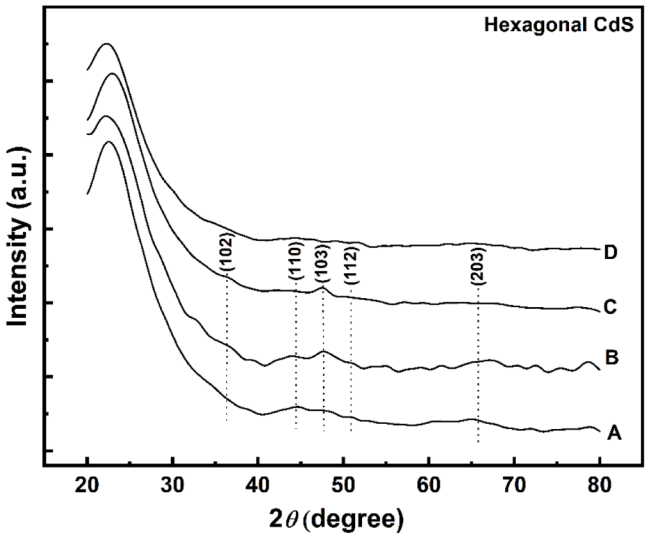

Fig. 3. XRD patterns of CdS-silica aerogels (A-C) and undoped silica aerogel (D).

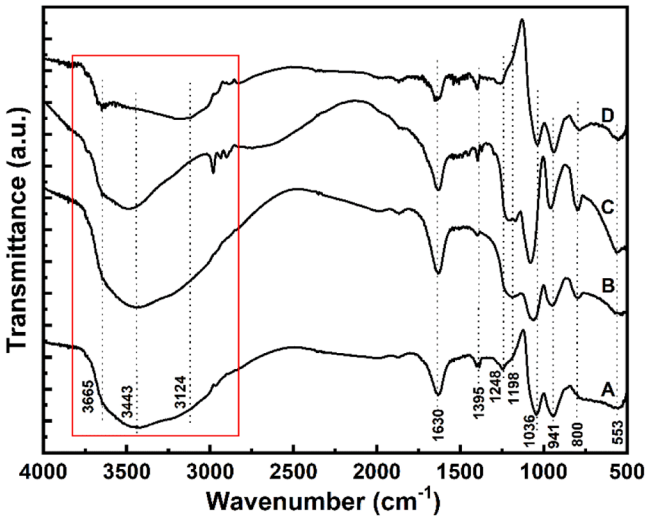

Fig. 4. FTIR spectra of CdS-silica aerogels (A-C) and undoped silica aerogel (D).

the 3000–3700 cm^{-1} region (highlighted in the red rectangle in Fig. 4) suggest the presence of non-covalent interactions, including Van der Waals forces and hydrogen bonding. A peak at 3665 cm^{-1}, attributed to Si-OH stretching vibrations, appears in all samples but with varying intensities: it is more prominent in the undoped silica aerogel (sample D) and significantly weaker in the CdS-doped samples (A-C). This suggests that in the doped aerogels, Si-OH groups may be involved in non-covalent interactions with CdS nanoparticles, rather than remaining as free hydroxyl groups [9,34,35]. A strong absorption band at 3443 cm^{-1} is observed in all CdS-doped samples (A-C) but is absent in the undoped silica aerogel. This band corresponds to O—H stretching vibrations and is indicative of hydrogen bonding between the silica matrix and CdS

Table 2
Elemental analysis of CdS-doped and undoped silica aerogel samples.

Aerogel	Drying	Cd (at. %)	S (at. %)	Si (at. %)	O (at. %)	Na (at. %)	Cd:S ratio
A) CdS-silica aerogel	Subcritical (Conc. C1)	50.96	49.04	-	-	-	1:1
B) CdS-silica aerogel	Subcritical (Conc. C2)	70.04	29.96	-	-	-	2:1
C) CdS-silica aerogel	Supercritical (Conc. C1)	48.71	51.29	-	-	-	1:1
D) Silica aerogel	Subcritical	0.13	0.06	27.74	58.94	10.17	-

Table 3
Mid-infrared FTIR analysis results of CdS-doped and undoped silica aerogel samples. Peak intensities are denoted as w = weak, m = moderate, s = strong, and nil = no peak observed.

Peak no.	Peak position (cm^{-1})				Peak assignment (bonding vibrations)
	Sample A	Sample B	Sample C	Sample D	
1	3665, w	3665, w	3665, w	3665, m	Si-OH stretching
2	3443, s	3443, s	3486, s	nil	O-H stretching from water
3	3124, w	3124, w	nil	3124, m	Hydrogen bonding
4	1630, s	1630, s	1630, s	1630, m	Si—O stretching, O—H bending
5	1395, m	1395, w	1395, m	1395, m	O-Si-O unsymmetric stretching
6	1198, w	1198, m	1198, m	nil	Si-S-Si streching
7	941, s	941, s	955, s	941, s	Si-OH bending
8	800, w	800, m	800, s	800, w	Si-O-Si bending, Si-C stretching
9	560, m	560, m	560, m	541, w	Cd-S streching

nanoparticles. Furthermore, a peak at 3124 cm^{-1}, present with moderate intensity in sample D, appears with reduced intensity in subcritically dried CdS-doped samples (A and B) and is absent in the supercritically dried sample (C). This suggests that subcritical drying retains hydrogen-bonded silanol groups and trace ethanol, while supercritical drying eliminates such interactions due to ethanol removal at supercritical temperatures.

The PL spectra of the CdS-silica aerogels (A-C) and of the undoped silica aerogel (D) are presented in Fig. 5. It is observed that the subcritically dried silica aerogel (sample D) does not exhibit any emission. In contrast, the CdS-doped silica aerogels (samples A-C) display four distinct emission bands at 470 nm (blue), 520 and 592 nm (green), and 673 nm (red) in the PL spectra. The excitation wavelength and emission filter were set at 380 and 390 nm, respectively, and these parameters were kept constants for all the samples.

The PL spectra of CdS nanoparticles typically consist of two broad bands: a high-energy band at the band-edge spectral energies and a low-energy band in the near-infrared (NIR) to red spectral range [15,16]. The high-energy band (band-edge) emission is attributed to various recombination mechanisms, such as the recombination of delocalized electron-hole (e-h) pairs strongly coupled to lattice vibrations or recombination through localized states, primarily of surface origin. The low-energy band, on the other hand, is associated with donor-acceptor

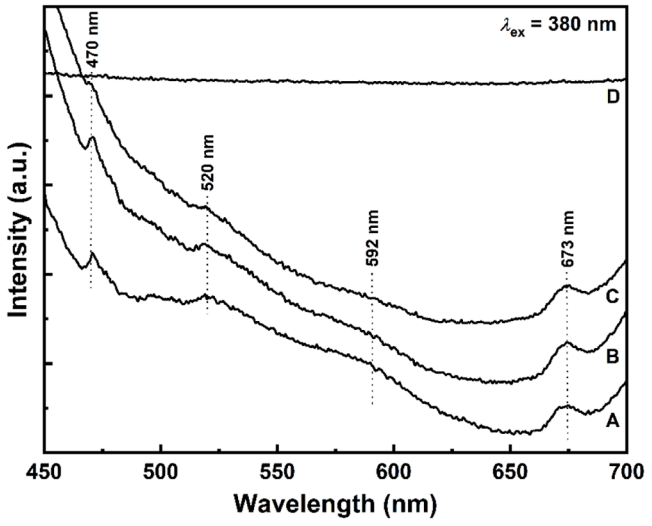

Fig. 5. Photoluminescence spectra of CdS-silica aerogels (A-C) and undoped silica aerogel (D) using an excitation wavelength of λ = 380 nm.

recombination involving deep defect states, such as sulfur vacancies (V_S) [36].

More in detail, the PL of CdS nanocrystals is primarily associated with the recombination of trapped electrons and holes at surface defects (traps). Upon photoexcitation, the generated holes can migrate to the surface of the CdS nanocrystals, forming sulfur (S^{2-}) traps. These traps are reported to exist approximately 1.5 eV above the valence band [31]. The recombination of photo-generated electrons, either from the conduction band or from electron traps, with holes at S^{2-} traps competes with the more efficient hole transfer processes, resulting in weak emission. It has been suggested that such S^{2-} traps are absent in CdS clusters with Cd^{2+}-rich centers. Additionally, surface defects can also arise from cation vacancies (Cd^{2+}), referred to as V^{2+} defects. These V^{2+} vacancies are reported to be located approximately 0.7 eV below the conduction band of CdS clusters [31].

Our study demonstrates that colloidal CdS nanoparticles, prior to incorporation into the silica matrix, exhibit a single blue emission band centered at around 470 nm (Fig. 1), characteristic of surface trap states. However, upon embedding the nanoparticles into the silica aerogel matrix, the PL spectrum broadens significantly to include distinct emission bands in the blue (470 nm), green (520 and 592 nm), and red (673 nm) regions (Fig. 5). This spectral evolution indicates the generation of additional defect states, which can be attributed to interactions between the nanoparticles and the aerogel environment. Specifically, the green and red emissions are associated with sulfur and cation vacancies, respectively; the red band, in particular, is likely related to deep-level defect states arising from site substitution phenomena. Control experiments with undoped silica aerogels (sample D) showed no measurable PL response, confirming that the observed emissions are intrinsic to the embedded CdS nanoparticles. The PL spectra exhibited consistent emission bands across all regions of the samples, indicating spatial uniformity in optical properties.

The green emission bands at 520 and 592 nm are associated with sulfur vacancies (V_S) and cation vacancies (V^{2+}), respectively, which have also been reported for thiophenol-capped CdS nanocrystals [37]. In our CdS-doped silica aerogel samples (A-C), the strong green emission observed at 520 nm is attributed to cation (Cd^{2+}) defects located 0.7 eV below the conduction band, while the weak emission at 592 nm is assigned to S^{2-} traps located 1.5 eV above the valence band.

The red emission observed at 673 nm, originating from the CdS nanoparticles in the CdS-doped silica aerogel, has been rarely studied. However, red emission from uncapped CdS nanoparticles has been reported at 1.9 eV by Fernandez et al. [38]. Additionally, Martínez-Castañón et al. [39] observed red emission at 660 nm from water-soluble CdS nanocrystals. The origin of the red emission can be explained using the site substitution model [31], which suggests that traps are generated by substituting sulfur ions with other counter ions. This process may involve the pairing of a Cd vacancy (V_{Cd}) with substitutional oxygen (O) or nitrogen (N) ions on adjacent sulfur sites. Consequently, a complex center, $V_{Cd\text{-}O}$ or $V_{Cd\text{-}N}$, is formed, consisting of a Cd vacancy and an O or N ion. Holes can be trapped at this center through nonradiative processes and subsequently recombine with electrons in excited electronic states, giving rise to the red emission band at 673 nm.

Furthermore, comparison with literature reveals that CdS nanoparticles embedded in alternative host matrices—such as xerogels or polymers—typically exhibit simpler PL profiles, often dominated by band-edge or single defect-related emissions. For instance, prior studies involving CdS in polymer matrices or CdSe-ZnS heterostructures commonly report one or two emission peaks [40]. In contrast, the CdS-doped silica aerogels investigated in this work display a distinctive multi-band PL response. This complex emission behavior is attributed to the highly porous architecture and chemically active environment of the silica matrix, which not only spatially confines the nanoparticles but also modulates defect formation and carrier recombination pathways. To the best of our knowledge, such host-induced tuning of luminescence

in CdS-doped aerogels—achieved via our sol-gel synthesis and supercritical drying method—has not been previously reported.

Preliminary stability tests indicate that the PL characteristics of the CdS-doped aerogels remained largely unchanged over a period of up to one month. This stability is likely supported by the intrinsic properties of the silica matrix—specifically, its chemical inertness, low hygroscopicity, and mechanically robust porous framework—which collectively help shield the embedded CdS nanoparticles under mild environmental conditions.

Based on our experimental observations, the majority of the CdS nanoparticles embedded within the silica aerogel—particularly in the subcritically dried samples (A and B)—exhibit no evidence of significant aggregation or oxidation. This inference is supported by the retention of sharp and well-defined emission bands in the PL spectra, as well as the presence of distinct diffraction peaks in the XRD patterns, which confirm the persistence of the hexagonal crystalline structure of CdS. These findings suggest that the nanoparticles largely maintain their nanoscale dispersion and chemical integrity. The silica matrix plays a crucial role in this stability. Its highly porous yet chemically inert framework serves as a protective host that both physically confines the CdS nanoparticles and shields them from environmental oxidants. This confinement limits particle mobility, thereby minimizing the risk of aggregation, while also creating a diffusion barrier that reduces the probability of surface oxidation over time.

The morphology of the CdS-silica aerogels (A-C) and of the undoped silica aerogel (D) is shown in Fig. 6. The morphology of samples A and B is comparable to that of the subcritically dried silica aerogel (sample D). The silica network in the subcritically dried samples (A, B, and D) is observed to be more compact compared to the supercritically dried CdS-silica aerogel (sample C). The high compactness of the CdS-silica aerogels (A and B) supports the conclusion that CdS nanoparticles are well-integrated into the pores of the silica aerogel, without significant aggregation. In contrast, the highly porous structure of sample C is less effective at retaining the nanoparticles during supercritical drying, likely due to the following mechanisms:

- Non-covalent interactions and ligand stability: In our synthesis, thiolate-capped CdS nanoparticles are incorporated into the silica sol via non-covalent interactions, which help anchor them within the forming silica network. Under ambient drying, these interactions, in conjunction with the capillary forces present during solvent evaporation, are sufficient to retain a significant fraction of CdS nanoparticles. However, under supercritical drying, the conditions drastically change.
- Supercritical drying conditions and dynamic solvent effects: Supercritical drying is carried out at elevated temperatures (~260–265 °C) and pressures, where the solvent (ethanol) exists in a supercritical state with negligible surface tension. The resultant removal of capillary forces means that nanoparticles that are only weakly anchored—either by non-covalent interactions or through loose physical entrapment—are more susceptible to being mobilized and removed from the silica network. Additionally, the rapid kinetics associated with solvent extraction in the supercritical process may further contribute to the desorption of loosely retained CdS nanoparticles.
- Microstructural rearrangement of the silica network: The elevated temperature and pressure during supercritical drying can induce reorganization of the silica network, including pore expansion or morphological restructuring. Such changes may create pathways that allow loosely embedded CdS nanoparticles to migrate out of the porous matrix, particularly those not confined within smaller or more tortuous pore regions.

As reported above, our CdS-doped silica aerogels exhibit a unique multi-band PL profile, with distinct emission peaks in the blue (470 nm), green (520 and 592 nm), and red (673 nm) regions. This broad spectral coverage contrasts with many previously reported luminescent aerogel systems, such as those incorporating CdSe-ZnS core-shell nanoparticles or organic dyes, which typically exhibit single or dual emission bands [9,

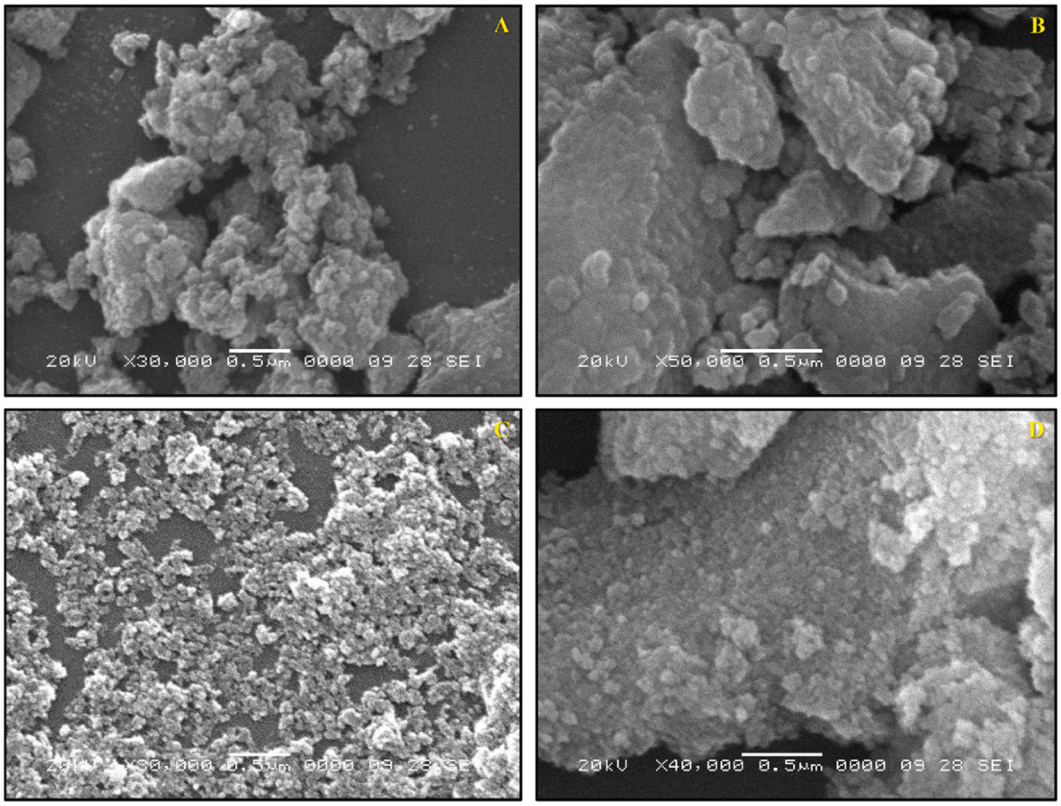

Fig. 6. SEM images of CdS-silica aerogels (A-C) and undoped silica aerogel (D).

39,40]. The presence of multiple emission centers in our system not only highlights the intrinsic defect states and surface traps of CdS nanoparticles but also offers clear advantages for applications requiring tunable or broadband light emission, such as white light-emitting diodes (LEDs), color displays, or optical sensors [39].

The simultaneous emission in the blue, green, and red regions enables the potential generation of white light through suitable spectral blending. By carefully tuning the relative intensities of these emission bands—via control over CdS nanoparticles concentration, drying conditions, or defect engineering—it should be possible to engineer a luminescent material that emits high-quality white light when excited by a UV or blue LED. The chemical and structural stability provided by the silica aerogel matrix further enhances the appeal of these materials for use in solid-state lighting, where long-term photostability and color consistency are critical. The observed multi-band PL also offers a pathway for constructing dynamic, multi-color display devices. Spatial or temporal modulation of the individual emission bands could be exploited to generate displays with a wide color range. Moreover, the ability to fine-tune the emission wavelengths by altering the defect state populations or nanoparticle surface characteristics might allow for the precise control of color output in advanced display technologies.

Beyond lighting and display applications, CdS nanoparticles luminescence is known to be sensitive to environmental factors such as humidity, gas exposure, and pH. In our system, variations in the local chemical environment can affect surface states and defect populations, which in turn modulate emission intensities and lifetimes. This sensitivity makes the aerogel composites strong candidates for optical sensors, where shifts in PL can be used as a readout for detecting specific analytes or monitoring ambient conditions.

4. Conclusions

In conclusion, CdS-doped silica aerogels, which were dried under two different conditions: at room temperature and at the supercritical temperature, were successfully synthesized. Supercritical drying of the CdS-doped aerogels resulted in the partial removal of QDs, indicating that the CdS nanoparticles are non-covalently bonded to the silica matrix. However, some QDs remained embedded in the aerogel, as evidenced by the weak emission bands observed in the PL spectra and the XRD patterns of the CdS-silica aerogel samples. The non-covalent interactions between CdS nanoparticles and silica aerogel are further supported by FTIR analysis. The PL study of the CdS-doped silica aerogels revealed three distinct emission bands: blue (470 nm), green (520 and 592 nm), and red (673 nm). The blue emission is attributed to localized trap states on the surface of the CdS nanoparticles, while the green emission is associated with sulfur vacancies (V_S) and cation vacancies (V^{2+}). The red emission is linked to the substitution of sulfur traps by other counter ions, as suggested by the site substitution model.

CRediT authorship contribution statement

Prashant B. Lihitkar: Writing – original draft, Methodology, Investigation, Funding acquisition, Data curation, Conceptualization. **Sonali Kale:** Visualization, Validation, Supervision, Methodology, Investigation, Conceptualization. **Rakesh A. Afre:** Writing – review & editing, Validation, Supervision, Formal analysis, Conceptualization. **Diego Pugliese:** Writing – review & editing, Validation, Supervision, Conceptualization.

Declaration of competing interest

The authors declare that they have no known competing financial interests or personal relationships that could have appeared to influence the work reported in this paper.

Acknowledgments

P. B. Lihitkar would like to thank Dr. S. K. Kulkarni for her valuable guidance. The Department of Physics of the Savitribai Phule Pune University (SPPU), Pune, India, and the Department of Science and Technology (DST), New Delhi, India, are also acknowledged for their infrastructure and financial support to pursue the present research work.

Data availability

Data will be made available on request.

References

[1] A.C. Pierre, G.M. Pajonk, Chemistry of aerogels and their applications, Chem. Rev. 102 (2002) 4243–4266, https://doi.org/10.1021/cr0101306.
[2] B.T. Mekonnen, W. Ding, H. Liu, S. Guo, X. Pang, Z. Ding, M.H. Seid, Preparation of aerogel and its application progress in coatings: a mini overview, J. Leather Sci. Eng. 3 (2021) 25, https://doi.org/10.1186/s42825-021-00067-y.
[3] M. Borzova, K. Schollbach, F. Gauvin, H.J.H. Brouwers, Sustainable ambient pressure-dried silica aerogel from waste glass, Curr. Res. Green Sustainable Chem. 9 (2024) 100425, https://doi.org/10.1016/j.crgsc.2024.100425.
[4] T. Kodanek, A. Freytag, A. Schlosser, S. Naskar, T. Härtling, D. Dorfs, N.C. Bigall, Macroscopic aerogels with retained nanoscopic plasmonic properties, Z. Phys. Chem. 232 (2018) 1675–1689, https://doi.org/10.1515/zpch-2017-1045.
[5] A.-G. Niculescu, D.-I. Tudorache, M. Bocioagă, D.E. Mihaiescu, T. Hadibarata, A. M. Grumezescu, An updated overview of silica aerogel-based nanomaterials, Nanomaterials 14 (2024) 469, https://doi.org/10.3390/nano14050469.
[6] L. Zhao, L. Zhu, L. Liu, J. Zhang, Y. Li, B. Zhang, J. Shen, J. Wang, Cluster generation from doped silica aerogels by XeCl excimer laser ablation, Chem. Phys. Lett. 255 (1996) 142–146, https://doi.org/10.1016/0009-2614(96)00344-2.
[7] Y. Wu, X. Wang, L. Liu, Z. Zhang, J. Shen, Alumina-doped silica aerogels for high-temperature thermal insulation, Gels 7 (2021) 122, https://doi.org/10.3390/gels7030122.
[8] S.K. Sharma, P. Ranjani, H. Mamane, R. Kumar, Preparation of graphene oxide-doped silica aerogel using supercritical method for efficient removal of emerging pollutants from wastewater, Sci. Rep. 13 (2023) 16448, https://doi.org/10.1038/s41598-023-43613-w.
[9] S. Dervin, Y. Lang, T. Perova, S.H. Hinder, S.C. Pillai, Graphene oxide reinforced high surface area silica aerogels, J. Non-Cryst. Solids 465 (2017) 31–38, https://doi.org/10.1016/j.jnoncrysol.2017.03.030.
[10] P. Zhao, B. Jin, J. Yan, R. Peng, Fabrication of recyclable reduced graphene oxide/graphitic carbon nitride quantum dot aerogel hybrids with enhanced photocatalytic activity, RSC Adv 11 (2021) 35147–35155, https://doi.org/10.1039/D1RA06347B.
[11] G. Lazovski, G. Bar, B. Ji, N. Atar, U. Banin, R. Gvishi, A simple method for preparation of silica aerogels doped with monodispersed nanoparticles in homogeneous concentration, J. Supercrit. Fluids 159 (2020) 104496, https://doi.org/10.1016/j.supflu.2019.03.008.
[12] Z. Yi, T. Jiang, Y. Cheng, Q. Tang, Effect of SiO_2 aerogels loading on photocatalytic degradation of nitrobenzene using composites with tetrapod-like ZnO, Nanotechnol. Rev. 9 (2020) 1009–1016, https://doi.org/10.1515/ntrev-2020-0081.
[13] L. Sorensen, G.F. Strouse, A.E. Stiegman, Fabrication of stable low-density silica aerogels containing luminescent ZnS capped CdSe quantum dots, Adv. Mater. 18 (2006) 1965–1967, https://doi.org/10.1002/adma.200600791.
[14] S. Rai, L. Bokatial, Effect of CdS nanoparticles on photoluminescence spectra of Tb^{3+} in sol–gel-derived silica glasses, Bull. Mater. Sci. 34 (2011) 227–231, https://doi.org/10.1007/s12034-011-0084-6.
[15] J. Mu, L. Xu, Q. Wei, Influence of CdS nanoparticles on the photoluminescence of silica xerogel, J. Dispersion Sci. Technol. 27 (2006) 171–173, https://doi.org/10.1080/01932690500265847.
[16] N. De La Rosa-Fox, M. Piñero, R. Litrán, L. Esquivias, Photoluminescence from CdS quantum dots in silica gel, J. Sol-Gel Sci. Technol. 26 (2003) 947–951, https://doi.org/10.1023/A:1020796910452.
[17] F. Ben Slimen, Z. Zaaboub, M. Haouari, N. Bel Haj Mohamed, H. Ben Ouada, S. Chaussedent, N. Gaumer, Effect of CdS nanocrystals on the photoluminescence of Eu^{3+}-doped silicophosphate sol gel glass, RSC Adv. 7 (2017) 14552–14561, https://doi.org/10.1039/C7RA01313B.
[18] L. Bokatial, S. Rai, Photoluminescence and energy transfer study of Eu^{3+} codoped with CdS nanoparticles in silica glass, J. Fluoresc. 22 (2012) 505–510, https://doi.org/10.1007/s10895-011-0984-2.
[19] Z. Pei, H. Guo, L. Zhu, C. Li, Z. Fu, J. Xu, Photocatalytic degradation of various antibiotics under visible light irradiation by CdS-doped SiO_2@BiOX (X = Br, Cl) prepared by mixed solvothermal method, Mater. Sci. Eng. B 287 (2023) 116134, https://doi.org/10.1016/j.mseb.2022.116134.
[20] N. Fatemipayam, N. Keramati, M.M. Ghazi, Synthesis and characterization of cadmium sulfide and titania photocatalysts supported on mesoporous silica for optimized dye degradation under visible light, Sci. Rep. 15 (2025) 8160, https://doi.org/10.1038/s41598-025-92077-7.
[21] J. Kaushik, V.K. Himanshi, K.M. Tripathi, S.K. Sonkar, Sunlight-promoted photodegradation of Congo red by cadmium-sulfide decorated graphene aerogel,

Chemosphere 287 (2022) 132225, https://doi.org/10.1016/j.chemosphere.2021.132225.
[22] J.L. Mohanan, S.L. Brock, A new addition to the aerogel community: unsupported CdS aerogels with tunable optical properties, J. Non-Cryst. Solids 350 (2004) 1–8, https://doi.org/10.1016/j.jnoncrysol.2004.05.020.
[23] S. Prasad, P. Shanmugam, K. Bhuvaneswari, G. Palanisamy, T. Pazhanivel, T. Arunkumar, M.S. AlSalhi, M.J. Aljaafreh, Rod-shaped carbon aerogel-assisted CdS nanocomposite for the removal of methylene blue dye and colorless phenol, Crystals 10 (2020) 300, https://doi.org/10.3390/cryst10040300.
[24] H. Yang, L. Jiang, W. Wang, Z. Luo, J. Li, Z. He, Z. Yan, J. Wang, One-pot synthesis of CdS/metal–organic framework aerogel composites for efficient visible photocatalytic reduction of aqueous Cr(VI), RSC Adv. 9 (2019) 37594–37597, https://doi.org/10.1039/C9RA08339A.
[25] M. Ikram, M. Naz, A. Haider, I. Shahzadi, H.U. Mehboob, M.A. Bari, A. Ul-Hamid, M.M. Algaradah, M.M. Al-Anazy, Carbon sphere doped CdS quantum dots served as a dye degrader and their bactericidal behavior analysed with *in silico* molecular docking analysis, Nanoscale Adv. 6 (2024) 233–246, https://doi.org/10.1039/D3NA00579H.
[26] J.L. Mohanan, I.U. Arachchige, S.L. Brock, Porous semiconductor chalcogenide aerogels, Science 307 (2005) 397–400, https://doi.org/10.1126/science.1104226.
[27] T. Gacoin, K. Lahlil, P. Larregaray, J.-P. Boilot, Transformation of CdS colloids: sols, gels, and precipitates, J. Phys. Chem. B 105 (2001) 10228–10235, https://doi.org/10.1021/jp011738l.
[28] S. Bag, I.U. Arachchige, M.G. Kanatzidis, Aerogels from metal chalcogenides and their emerging unique properties, J. Mater. Chem. 18 (2008) 3628–3632, https://doi.org/10.1039/B804011G.
[29] H. Tang, M. Yan, H. Zhang, M. Xia, D. Yang, Preparation and characterization of water-soluble CdS nanocrystals by surface modification of ethylene diamine, Mater. Lett. 59 (2005) 1024–1027, https://doi.org/10.1016/j.matlet.2004.11.049.
[30] T. Torimoto, H. Kontani, Y. Shibutani, S. Kuwabata, T. Sakata, H. Mori, H. Yoneyama, Characterization of ultrasmall CdS nanoparticles prepared by the size-selective photoetching technique, J. Phys. Chem. B 105 (2001) 6838–6845, https://doi.org/10.1021/jp0109271.
[31] B. Liu, G.Q. Xu, L.M. Gan, C.H. Chew, W.S. Li, Z.X. Shen, Photoluminescence and structural characteristics of CdS nanoclusters synthesized by hydrothermal microemulsion, J. Appl. Phys. 89 (2001) 1059–1063, https://doi.org/10.1063/1.1335642.
[32] G.Q. Xu, B. Liu, S.J. Xu, C.H. Chew, S.J. Chua, L.M. Gana, Luminescence studies of CdS spherical particles via hydrothermal synthesis, J. Phys. Chem. Solids 61 (2000) 829–836, https://doi.org/10.1016/S0022-3697(99)00403-5.
[33] A. Lesiak, B. Wagnon, D. Chateau, B. Abécassis, S. Parola, Room temperature synthesis of CdSe/CdS triangular nanoemitters and their stabilization in colloidal state and sol–gel glass, RSC Adv. 13 (2023) 28407–28415, https://doi.org/10.1039/D3RA04992B.
[34] G. Murugadoss, R. Thangamuthu, R. Jayavel, M.R. Kumar, Narrow with tunable optical band gap of CdS based core shell nanoparticles: applications in pollutant degradation and solar cells, J. Lumin. 165 (2015) 30–39, https://doi.org/10.1016/j.jlumin.2015.03.036.
[35] K. Kandasamy, M. Venkatesh, Y.A.S. Khadar, P. Rajasingh, One-pot green synthesis of CdS quantum dots using *Opuntia ficus-indica* fruit sap, Mater. Today Proc. 26 (2020) 3503–3506, https://doi.org/10.1016/j.matpr.2019.06.003.
[36] V. Klimov, P.H. Bolivar, H. Kurz, Ultrafast carrier dynamics in semiconductor quantum dots, Phys. Rev. B 53 (1996) 1463–1467, https://doi.org/10.1103/PhysRevB.53.1463.
[37] A. Datta, A. Priyam, S.N. Bhattacharyya, K.K. Mukherjea, A. Saha, Temperature tunability of size in CdS nanoparticles and size dependent photocatalytic degradation of nitroaromatics, J. Colloid Interface Sci. 322 (2008) 128–135, https://doi.org/10.1016/j.jcis.2008.02.052.
[38] J.R.L. Fernandez, M. De Souza-Parise, P.C. Morais, Optical investigation of the red band emission of CdS nanoparticles, Surf. Sci. 601 (2007) 3805–3808, https://doi.org/10.1016/j.susc.2007.04.149.
[39] G.A. Martínez-Castañón, M.G. Sánchez-Loredo, J.R. Martínez-Mendoza, F. Ruiz, Synthesis of CdS nanoparticles: a simple method in aqueous media, Adv. Technol. Mater. Mater. Process. J. 7 (2005) 171–174.
[40] B. Xu, T. Zhang, X. Lin, H. Yang, X. Jin, Z. Huang, Z. Zhang, D. Li, Q. Li, One pot synthesis of thick shell blue emitting CdZnS/ZnS quantum dots with narrow emission line width, Opt. Mater. Express 10 (2020) 1232–1240, https://doi.org/10.1364/OME.389823.